International Journal of the Physical Sciences Vol. 5(6), pp. 690-695, June 2010
Available online at http://www.academicjournals.org/IJPS
ISSN 1992 - 1950 © 2010 Academic Journals

Full Length Research Paper

Calculated electron steady-state drift velocity in lattice matched $Ga_{0.5}In_{0.5}P$ and $Al_{0.26}Ga_{0.26}In_{0.48}P$ using a three-valley Monte Carlo simulation

S. Golafroz* and H. Arabshahi

Department of Physics, Ferdowsi University of Mashhad, Mashhad, Iran.

Accepted 6 April, 2010

We present calculations based on an ensemble Monte Carlo program of the steady-state electron drift velocity in bulk $Ga_{0.5}In_{0.5}P$ and $Al_{0.26}Ga_{0.26}In_{0.48}P$ as well as present a list of material parameters for these substances which are of use in the modeling of semiconductor devices made from these material types. Calculations are made using a non-parabolic effective mass energy band model, Monte Carlo simulation that includes all of the major scattering mechanisms. The band parameters used in the simulation are extracted from optimized pseudopotential band calculations to ensure excellent agreement with experimental information and *ab-initio* band models. The effects of alloy scattering on the electron transport physics are examined. For two materials, it is found that electron velocity overshoot only occurs when the electric field is increased to a value above a certain critical field, unique to each material. This critical field is strongly dependent on the material parameters.

Key words: Steady-state, pseudopotential, alloy scattering, velocity overshoot, critical field.

INTRODUCTION

The quaternary semiconductor, $Al_{0.26}Ga_{0.26}In_{0.48}P$ offers the largest direct band gap of the 3 - 5 compound semiconductor material which is lattice matched to a commonly available substrate (Brennan, 1983). Owing to its relatively large band gap, this material has been cited for its potential use in visible light emitters such as light emitting diodes and lasers (Newman et al., 1985, 1986). $Al_{0.26}Ga_{0.26}In_{0.48}P$ has further potential usage as a visible light detector as well as in high temperature and/or high power electronics. The additional advantage of being lattice matched to the ternary compound $Ga_{0.5}In_{0.5}P$ as well as GaAs offers large flexibility in the choice of heterostructures which can be made from this material. To date, a GaInP/AlGaInP double heterostructure laser grown on a GaAs substrate has been successfully demonstrated at room-temperature cw operation. Improved electron transport properties are one of the main targets in the ongoing study of ternary and quaternary $Ga_{0.5}In_{0.5}P$ and $Al_{0.26}Ga_{0.26}In_{0.48}P$ materials.

*Corresponding author. E-mail: arabshahi@um.ac.ir.

The Monte Carlo technique has proved valuable for studying non-equilibrium carrier transport in a range of semiconductor materials and devices (Cameron et al., 1983 - 1984). However, carrier transport modeling of $Ga_{0.5}In_{0.5}P$ and $Al_{0.26}Ga_{0.26}In_{0.48}P$ materials has only recently begun to receive sustained attention, now that the growth of compounds and alloys is able to produce valuable material for the electronics industry. To clarify the expected performance of these materials, transport as well as device studies are critical. Thus, it is the purpose of this paper to compare steady-state and transient velocity overshoot in $Ga_{0.5}In_{0.5}P$ and $Al_{0.26}Ga_{0.26}In_{0.48}P$ materials using an ensemble Monte Carlo studies. Our current approach employs a one-dimensional ensemble Monte Carlo technique to investigate steady-state and transient electron transport in $Ga_{0.5}In_{0.5}P$ and $Al_{0.26}Ga_{0.26}In_{0.48}P$. However, the momentum space treatment is three dimensional and the scattering events consider all three dimensions. Specifically, our model includes the three lowest valleys of the conduction band with non-parabolic. The Monte Carlo results are only as reliable as the input material parameters used in the simulation which are typically not all known with sharp

Table 1. Valley parameter selections for $Ga_{0.5}In_{0.5}P$ and $Al_{0.26}Ga_{0.26}In_{0.48}P$.

	$Ga_{0.5}In_{0.5}P$	$Al_{0.26}Ga_{0.26}In_{0.48}P$
m_Γ	0.015	0.11
m_L	0.242	0.435
m_x	0.61	0.318
α_Γ	10.09	11.71
α_L	7.62	5.58
Γ-X	0.217	0.05
Γ-L	0.125	0.042

precision. In order to use Monte Carlo techniques for semiconductor device simulation, it is of principle importance to determine a reliable set of input parameters for each material system studied. In general, one adjusts the lesser known parameters, those not directly measurable, in order to agree with experimental measurements of the velocity-field characteristic. The comparison to experimental measurements, when available, serves as a control on the Monte Carlo calculations. The effects of a particular device geometry on the calculations can then be completely isolated since any difference between the calculated bulk and device quantities must be due solely to the device geometry.

The Monte Carlo method provides an additional advantage in that it can be used as a theoretical laboratory in that parameters can be varied at will and their effects on observables assessed. The method provides a very powerful present herein a series of computer experiments in which the effects of variations in the polar optical phonon energy, dielectric constants, effective masses and central to satellite valley separation energy on the steady-state electron velocity-field relationship for $Ga_{0.5}In_{0.5}P$ and $Al_{0.26}Ga_{0.26}In_{0.48}P$ are determined. This article is organized as follows. Details of the conduction band parameters and the Monte Carlo simulation are presented in section 2 and the results of steady-state and transient transport simulations are discussed in section 3.

MODEL DETAILS

Our ensemble Monte Carlo simulations of electron transport in zincblende $Ga_{0.5}In_{0.5}P$ and $Al_{0.26}Ga_{0.26}In_{0.48}P$ are similar to those of Arabshahi et al., (2007); Arabshahi, (2007). As indicated earlier, a three-valley model for the conduction band is employed.

In order to calculate the electron drift velocity for large electric fields, consideration of conduction band satellite valleys is necessary. The first-principles band structure of zincblende $Ga_{0.5}In_{0.5}P$ and $Al_{0.26}Ga_{0.26}In_{0.48}P$ predicts a direct band gap located at the Γ point and lowest energy conduction band satellite valleys at the *X* point and at the *L* point. In our Monte Carlo simulation, the Γ valley, the three equivalent *X* valleys, the four equivalent *L* valleys, are represented by ellipsoidal, non-parabolic dispersion relationships of the following form (Foutz et al., 1997; Bhapkar at al., 1997).

$$E(k)[1+\alpha_i E(k)] = \frac{\hbar^2 k^2}{2m^*} \quad (1)$$

Where m^* is effective mass at the band edge and α_i is the non-parabolic coefficient of the *i*-th valley given by Kane model (Kane, 1957) as

$$\alpha_i = \frac{1}{E_g}\left[1-\frac{2m^*}{m_0}\right]\left[1-\frac{E_g\Delta}{3(E_g+\Delta)(E_g+2\Delta/3)}\right] \quad (2)$$

Where E_g is the band-gap energy, Δ is the spin-orbit splitting and m_0 is the free electron effective mass.

We assume that all donors are ionized and that the free-electron concentration is equal to the dopant concentration. For each simulation, the motion of ten thousand electron particles are examined, the temperature being set to 300 K and the doping concentration being set to 10^{17} cm^{-3}. In the case of the ellipsoidal, non-parabolic conduction valley model, the usual Herring-Vogt transformation matrices are used to map carrier momenta into spherical valleys when particles are drifted or scattered. Electrons in bulk material suffer intra-valley scattering by polar optical, non-polar optical and acoustic phonons scattering, inter-valley phonons and ionized impurity scattering.

Acoustic scattering is assumed elastic and the absorption and emission rates are combined under the equipartition approximation, which is valid for lattice temperatures above 77 K. Elastic ionized impurity scattering is described using the screened Coulomb potential of the Brooks-Herring model. Band edge energies, effective masses and non-parabolic are derived from empirical pseudopotential calculations. Important parameters used throughout the simulations are listed in Tables 1-2.

In the case of $Ga_{0.5}In_{0.5}P$ and $Al_{0.26}Ga_{0.26}In_{0.48}P$ the alloy scattering has also been included. Alloy scattering refers to the scattering due to the random distribution of the component atoms of the alloy among the available lattice sites. Albrecht et al. (1998) assumed that the alloy crystal potential can be described as a perfectly periodic potential which is then perturbed by the local deviations from this potential, due to the disordering effects in the alloy. Using the Albrecht model, the scattering rate due to the chemical disorder in a ternary alloy of electrons in a non-parabolic band is given by (Moglestue, 1993; Jacoboni, 1989).

$$R_{alloy}(k) = \frac{4\sqrt{2}\pi m^{*3/2} r^6}{9\hbar^4}.\frac{x(1-x)\Delta U^2}{\Omega^2}\gamma^{1/2}(E)(1+2\alpha E) \quad (3)$$

Where $\gamma(E)$ is a function of electron energy, *x* denotes the molar fraction of one of the binary components of the alloy, Ω is the volume of the primitive cell and ΔU is the spherical scattering potential.

RESULTS

Figure 1 shows the simulated velocity-field characteristics of zincblende $Ga_{0.5}In_{0.5}P$ and $Al_{0.26}Ga_{0.26}In_{0.48}P$ semiconductors at 300 K, with a background doping concentration of 10^{17} cm^{-3} and with the electric field applied along one of the cubic axes. The simulations suggest that the peak drift velocity for zincblende $Al_{0.26}Ga_{0.26}In_{0.48}P$ is 1.4×10^5 ms^{-1}, while that for $Ga_{0.5}In_{0.5}P$ is about ~ 0.8×10^5 ms^{-1}. At higher electric fields, intervalley optical phonon emission dominates, causing

Table 2. Material parameter selections for $Ga_{0.5}In_{0.5}P$ and $Al_{0.26}Ga_{0.26}In_{0.48}P$.

	$Ga_{0.5}In_{0.5}P$	$Al_{0.26}Ga_{0.26}In_{0.48}P$
Density ρ (kgm^{-3})	4470	4010
Longitudinal sound velocity v_s (ms^{-1})	5490	5540
Low-frequency dielectric constant ε_s	11.75	11.49
High-frequency dielectric constant ε_∞	9.34	8.93
Acoustic deformation potential D(eV)	7.82	5.58
Polar optical phonon energy (eV)	0.046	0.049
Intervalley phonon energies (meV)	25.44	14.76

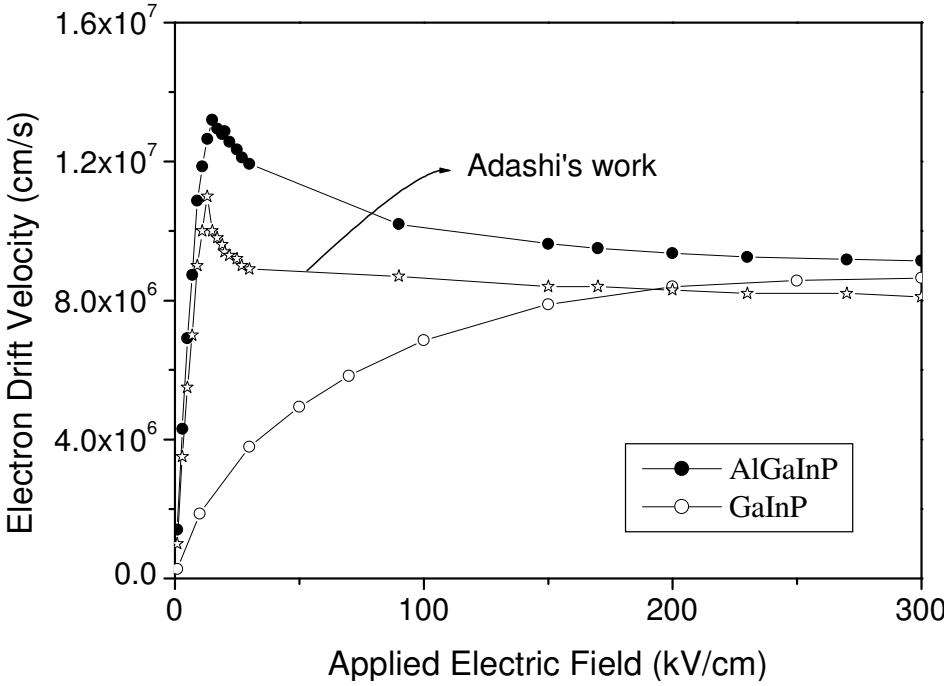

Figure 1. Calculated steady-state electron drift velocity in bulk zincblende $Ga_{0.5}In_{0.5}P$ and$Al_{0.26}Ga_{0.26}In_{0.48}P$ using non-parabolic band models at room temperature.

the drift velocity to saturate at around 0.9×10^4 ms^{-1} for two materials.

The calculated drift velocities apparent from Figure 1 are fractionally higher than those that have been calculated by Adachi et al. (1992, 1993, 1994), who assumed an effective mass in the upper valleys equal to the free electron mass. The threshold field for the onset of significant scattering into satellite conduction band valleys is a function of the intervalley separation and the density of electronic states in the satellite valleys.

The valley occupancies for the Γ, *X* and *L* valleys are illustrated in Figure 2 and show that the inclusion of the satellite valleys in the simulation is important. Significant intervalley scattering into the satellite valleys occurs for fields above the threshold field for each material. This is important because electrons which are near a valley minimum have small kinetic energies and are therefore strongly scattered. It is apparent that intervalley transfer is substantially larger in $Ga_{0.5}In_{0.5}P$ over the range of applied electric fields shown, due to the combined effect of a lower Γ effective mass, lower satellite valley separation energy and slightly lower phonon scattering rate within the Γ valley.

Figure 3 shows the calculated electron drift velocity as a function of electric field strength for temperatures of 300, 450 and 600 K. The decrease in drift mobility with temperature at low fields is due to increased intravalley polar optical phonon scattering whereas the decrease in velocity at higher fields is due to increased intra and intervalley scattering. It can be seen from the figure that the peak velocity also decreases and moves to higher electric field as the temperature is increased. This is due

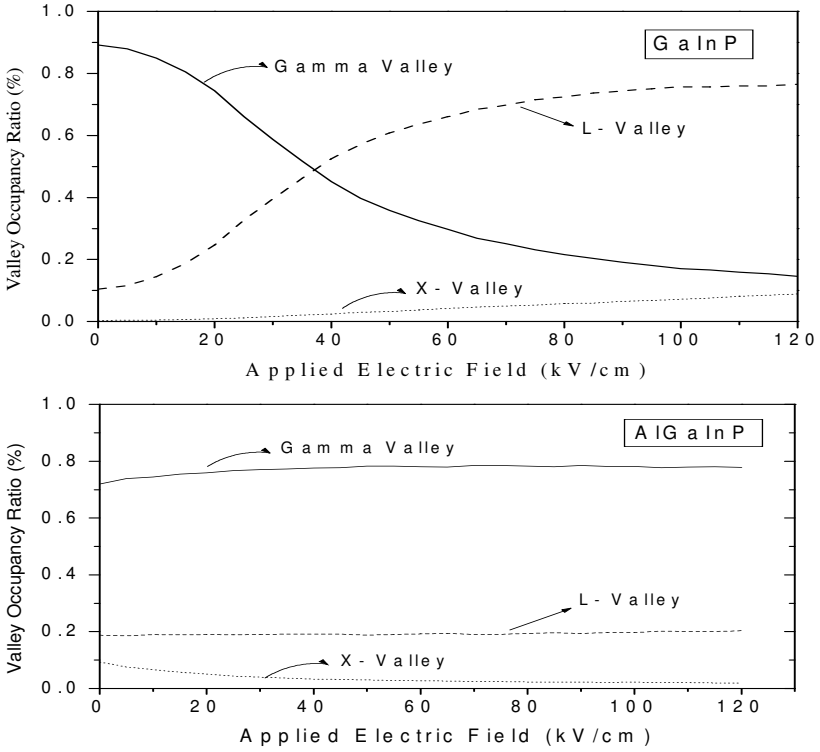

Figure 2. Fractional occupation of the central Γ and satellite valleys of zincblende $Ga_{0.5}In_{0.5}P$ and $Al_{0.26}Ga_{0.26}In_{0.48}P$ as a function of applied electric field using the non-parabolic band model at room temperature.

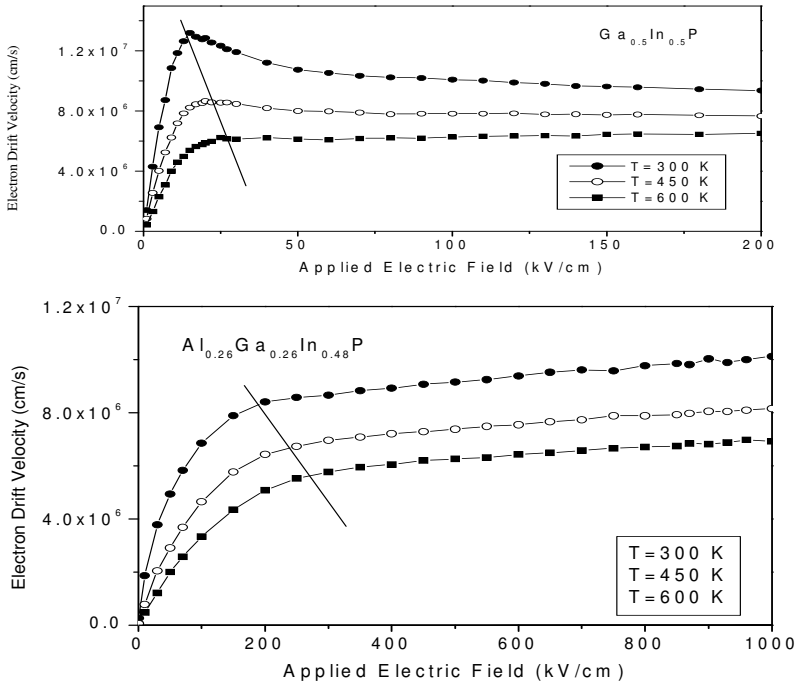

Figure 3. Calculated electron steady-state drift velocity in bulk zincblende $Ga_{0.5}In_{0.5}P$ and $Al_{0.26}Ga_{0.26}In_{0.48}P$ as a function of applied electric field at various lattice temperatures and assuming a donor concentration of 10^{17} cm^{-3}.

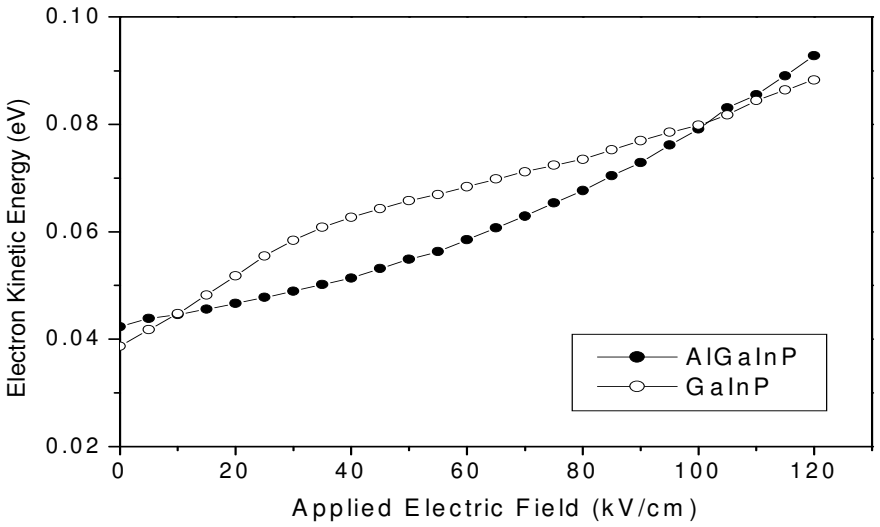

Figure 4. Average electron kinetic energy as a function of applied electric field in bulk zincblende $Ga_{0.5}In_{0.5}P$ and $Al_{0.26}Ga_{0.26}In_{0.48}P$ as a function of applied electric field using the non-parabolic band model at room temperature.

to the general increase of total scattering rate with temperature, which suppresses the electron energy and reduces the population of the satellite valleys. This latter effect is apparent from the fact that the electron population in the Γ valley increases with temperature as shown in Figure 2.

The average carrier kinetic energy as a function of electric field is shown in Figure 4. The curves have the S shape typical of 3 - 5 compounds, which is a consequence of intervalley transfer. At high fields, the curve for $Ga_{0.5}In_{0.5}P$ suggests that the average electron energy is higher than for $Al_{0.26}Ga_{0.26}In_{0.48}P$. This difference can be understood by considering the Γ-valley occupancy as a function of field (Figure 2). Intervalley transfer is substantially larger in the $Ga_{0.5}In_{0.5}P$, due to the combined effect of a lower Γ -valley effective mass, lower satellite valley separation and reduced phonon scattering rate within the Γ-valley, but significant intervalley phonon scattering at a threshold field of 500 kVm^{-1}. The peak drift velocity decreases by about 10% while the threshold field increases by same percent as the lattice temperature increases from 300 to 600 K.

Conclusions

Electron transport at 300 K in bulk zincblende $Ga_{0.5}In_{0.5}P$ and $Al_{0.26}Ga_{0.26}In_{0.48}P$ have been simulated using an ensemble Monte Carlo simulation. Using valley models to describe the electronic band structure, calculated velocity-field characteristics are in fair agreement with other calculations. Saturation drift velocities ~1.4×10^5 ms^{-1} match recent measurements on low-doped bulk samples. The velocity-field characteristics of the materials show similar trends, reflecting the fact that all the semiconductors have satellite valley effective densities of states several times greater than the central Γ valley. However, the peak velocity in $Ga_{0.5}In_{0.5}P$ occurs at a field ~ 25 kVm^{-1}, 6 times lower than for $Al_{0.26}Ga_{0.26}In_{0.48}P$. This is a consequence of the large Γ valley effective mass in $Al_{0.26}Ga_{0.26}In_{0.48}P$ structure.

ACKNOWLEDGEMENT

I would like to thank Maryam Gholvani Naeeini for her useful comments and writing up the paper.

REFERENCES

Adachi S (1992). Physical properties of 3-V Semiconductor Compounds, InP, InAs, GaAs, GaP,AlAs and AlGaAs, Wiley, New York.

Adachi S (1993). Properties of AlGaAs, INSPEC, Stevenage, Herts., UK.

Adachi S (1994) *GaAs* and Related Materials, Bulk semiconducting and Superlattice Properties, World Scientific, Singapore.

Albrecht JD, Wang RP, Ruden PP, Brennan KF (1998). Comparison of Transport Ballistic Electron Transport in Bulk Wurtzite Phase 6H-SiC and GaN, J. Appl. Phys., 83: 2185.

Arabshahi H, Benam MR, Salahi B (2007). A Shock-Capturing Upwind Disceritization Method For Characterization of SiC MESFETs, Modern Physics Letters B., 21: 1715.

Arabshahi H (2007). Monte Carlo Modeling of Hot Electron Transport in Bulk AlAs, AlGaAs and GaAs at Room Temperature, Modern Physics Letters B., 21: 199.

Bhapkar UV, Shur MS (1997). Temperature Dependence of High Field Electron Transport Properties in Wurtzite Phase GaN for Device, J. Appl. Phys., 82: 1649.

Brennan K, Hess K, Tang JY, Iafrate IG (1983) IEEE Trans. Electron Devices, 30: 1750.

Cameron DC, Irving LD, Whitehouse CR (1983). Comparison of High

and Low Field Electron Transport in AlGaN, AlN and GaN., Thin Solid Films., pp.103-161.
Cameron DC, Irving LD, Whitehouse CR (1982). Comparison of Low Field Electron Transport in SiC and GaN Structures for High-Power and high Temperature Device Modelling, Electron. Lett., pp.18, 534.
Foutz BE, Eastman LF, Bhapkar UV, Shur M (1997). Discretization Method of Hydrodynamic for simulation of GaN MESFETs. Appl. Phys. Lett., 70, 2849.
Jacoboni C, Lugli P (1989). The Monte Carlo Method for semiconductor and Device Simulation, Springer-Verlag.
Kane E O (1957). Computer Simulation of ZnO Field Effect Transistor for High-Power and High-Temperature Applications Using The Monte Carlo Method, J. Phys. Chem. Solids, 1: 249.
Moglestue C (1993). Monte Carlo Simulation of Semiconductor Devices, Chapman and Hall.
Newman N, Kendelewicz T, Bowman L, Spicer WE (1985). Effect of Various Material Parameters on the Calculated Velocity-field Relation in AlGaN at Room Temperature, Appl. Phys. Lett., pp. 46, 1176.
Newman N, Schilfgaarde T, Kendelewicz T, Spicer WE (1986). Low-Field Electron Transport Properties in Zincblende and Wurtzite GaN Structures Using an Iteration Model for Solving Boltzmann Equation Mater. Res. Soc. Symp. Proc., p. 54443.